www.czasopisma.pan.pl PAN POLSKA AKADEMIA NAUK www.journals.pan.pl

Arch. Metall. Mater. **68** (2023), 1, 195-204

DOI: https://doi.org/10.24425/amm.2023.141494

BÜNYAMIN ÇIÇEK[1*], YAVUZ SUN[2]

MATERIAL PRODUCTION AND THE EFFECT OF THE SYSTEM ON BIOCOMPATIBILITY IN THE MODIFIED METAL INJECTION METHOD

In this study, the bio state of the alloy produced in the modified metal injection system was monitored after sintering. A new system operating with high gas pressure, far from the traditional injection model, has been established for material production. In this system, 316L stainless steel powders were molded using a PEG/PMMA/SA polymer recipe. During molding, approximately 60% 316L and 40% binder by volume were used. The samples obtained were sintered at different temperatures (1100-1300°C) after de-binding. Density measurement (Archimedes) and hardness tests (HV1) of the samples were measured as 6.74 g/cm^3 and ~285 HV_1, respectively. A potentiodynamic corrosion test was applied to monitor the effect of the amount of oxide in the structure of the 316L stainless steel produced. Corrosion tests were carried out in artificial body solutions. The corrosion rate was measured at the level of 17.08×10^{-3} mm/y. In terms of biocompatibility, a cytotoxicity test was applied to the samples and the life course of the bacteria was monitored. For the 316L alloys produced, the % vitality reached approximately 103%.

Keywords: Metal Injection Molding; Stainless steel; polymer; biomaterial; cytotoxicity

1. Introduction

It is an accepted production method to turn particles into materials with the basic logic of powder metallurgy (PM) [1]. Particulate metals with different chemical content become metallic by molding with different methods [2]. At this stage, molding and sintering process are the most important variables. Particle structures with different alloys are mixed by many methods. Then, sintering is done at a specified temperature and atmosphere. The most important positive aspect of the PM production method is the geometric structure of complex materials, easier to produce [1,3,4].

Metal injection molding (MIM) method derived from PM method gives similar results in practice and industry [5,6]. In this method, a polymer structure is helped to make the particulate structures fluid. High volumetric particulate metals added to a particular polymer gel structure are transferred to a mold by different methods. The materials are transformed into metallic structure with a sintering process that needs to be controlled afterwards. Magnesium, stainless steel, Co-Cr-Mo and aluminum alloys are produced with this method (MIM) in recent years [7,8].

Metals have been preferred as implant materials for many years [9]. Developing material science has achieved important results for implant materials. At this stage, the functions and toxic effects of metallic structures added to the body for any reason should be known [10,11]. It is a current approach that discusses the effects of elements on the body. Cr and Ni alloys are used because of their high corrosion resistance [12,13]. Elements such as Mg and Zn are used as biodegradable [14,15]. In addition, the elements used are non-toxic structures [14-19]. The most common materials used as implants in the bio-material are stainless steel, Ti, Co-Cr-Mo and Mg alloys [20,21]. In addition, it is known that the bone structure is too complex to be produced by any metal processing method. Therefore, the production method of this type of orthopedic implants also requires special processes [20,22,23]. PM and its derivatives are the main production methods for orthopedic implants. Thus, materials that do not cause toxic effects and have complex geometric structures produced [22].

Formability is important in implant materials produced with PM. Therefore, MIM-like methods have been developed. With the high fluidity obtained from a polymer mixture, metal powders transferred to complex molds. At this stage, the

[1] HITIT UNIVERSITY, VOCATIONAL SCHOOL OF TECHNICAL SCIENCES, MACHINE AND METAL TECHNOLOGIES DEPARTMENT, CORUM, TURKEY
[2] KARABUK UNIVERSITY, ENGINEERING FACULTY, TURKEY
* Corresponding author: cicekbunyamin78@gmail.com

components of the polymer structure and the geometric forms of the powder metals are important. A successful MIM production made by controlling these parameters [1,5,6]. However, there are polymer-based C and O residues remaining in the structure during the sintering phase. These unwanted elements in the structure eliminated with some steps in the sintering process. As a result, implant materials are produced from alloys that will not cause toxic effects [3,4,24]. Due to the complex shape of the bone outer surface and internal structure, orthopedic implants generally become the final product with the MIM method [25,26]. Therefore, it is an important process to see the effect of residual oxide amount in the material produced in the system on biocompatibility. Already a bio-alloy, 316L stainless steel was used to study the full effect of the amount of oxide.

In this study, 316L particles, a stainless-steel alloy, and Polyethylene glycol 4000 (PEG) + Poly methyl methacrylate (PMMA) polymers were used. A newly designed MIM system was prepared at the stage of production method. As in our previous studies, MIM was performed with the help of high (Ar / 40 bar) gas pressure instead of hydraulic or screw type pressure [27,28]. The produced MIM parts are sintered (in Ar flow atmosphere) at different temperatures (1100 to 1300°C). The effect of polymer components on the obtained microstructures (with Scanning Electron Microscope-SEM) was followed. Potentiodynamic (Gamry 1010E) corrosion test was applied in artificial body, saliva, and NaCl solutions in samples with a metallic structure. In addition, a cytotoxicity test was applied to metallic structures. Thus, the biocontrol of the material produced in a newly developed method and the use of the system in the field of biomaterials are interpreted.

2. Materials and methods

2.1. Feedstock preparing

In the MIM production method, 316L quality stainless steel particles (D_{90}-18 µm) (Nanografi Co. Ltd in Turkey) are used to produce the feedstock (FS) structure. An FS structure was obtained with polymer binders for 316L whose chemical content is given in TABLE 1. PEG_{4k} (wt. 60%) and PMMA (wt. 35%) were used as the polymer structure (Polivin Chemistry and Petkim in Turkey). Stearic acid (SA) (wt. 5%) was added to the polymer recipe as a lubricant and plasticizer [29] (Sigma Aldrich in US). PEG ($C_{2n}H_{4n+2}O_{n+1}$): it was used as the main polymer in the structure as a filler. PMMA ($(C_5O_2H_8)_n$), on the other hand, served as the secondary polymer and skeletal structure [27,30,31]. The FS structure contains approximately 60% 316L and 40% polymer binders by volume. This ratio corresponds to approximately 92% and 8% by weight, respectively. SEM images of the raw materials used are given in Fig. 1.

Within the particle/polymer ratio given in TABLE 2, an FS structure has been prepared according to the basic principles in Fig. 2.

316L particles were dissolved physically in ethanol and then dried on hydrophobic paper (70°C/24 h). Later, the particles added into the liquid polymer structure (185°C) were homogenized in the sigma-blade mixing unit (170°C/0.5 h). Finally, it has been pelleted in irregular geometric structures with a diameter of approximately 10 mm. Thermal gravimetric analysis (TGA) was applied for FS and polymer ratio was monitored.

TABLE 1

316L chemical composition

Element	C	Cr	Ni	Mn	Mo	Si	P	S	N	Fe
wt. %	0.065	18.687	10.935	0.625	2.407	0.917	0.038	0.031	0.109	Balance

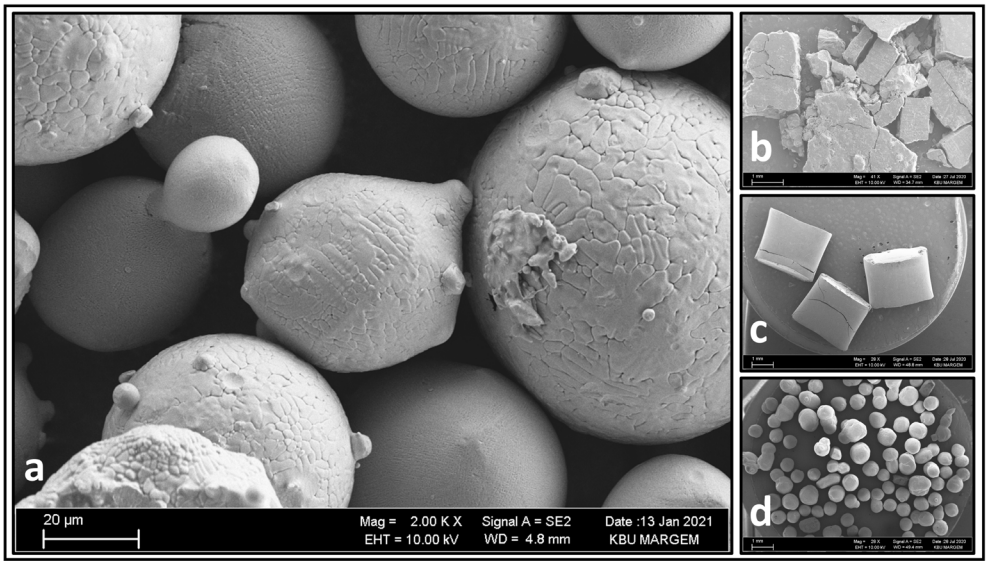

Fig. 1. SEM images; (a) 316L, (b) PEG, (c) PMMA, and (d) SA

TABLE 2

MIM parts components

Component	Metal Injection Molding (MIM) Parts			
	Binders (avg. dens. 1.17 gr/cm^3) vol. ~% 40			vol. ~% 60
	60% (wt)	35% (wt)	5% (wt)	Powder
	Main (filler binder)	Secondary (stuffy binder)	Lubricator	
Material	PEG	PMMA	SA	316L

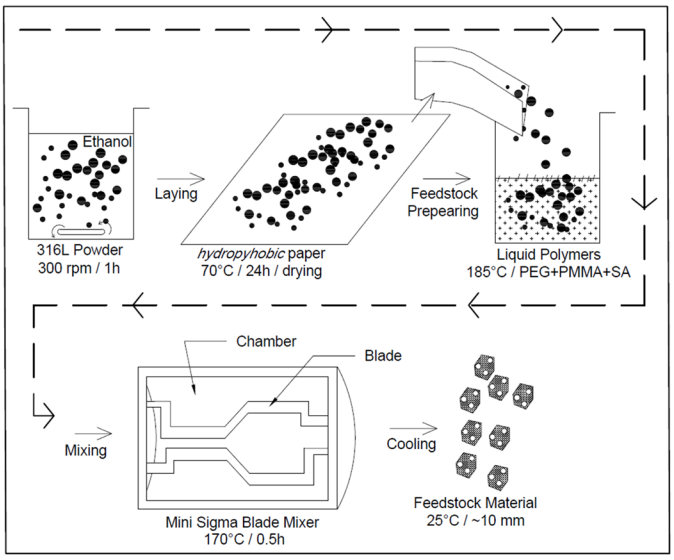

Fig. 2. Feedstock preparing process

2.2. Modified MIM, molding, and sintering

In the system prepared based on the idea of MIM, the mechanism shown in Fig. 3 has been established. Based on the results of our previous studies, a molding process was carried out with high Ar (99.9% pure) gas pressure (40 bar) [26,27]. In this molding process, the FS structure was brought into a gel form (180°C) in a melting chamber. Then, the gel structure passing through a nozzle (Ø4 mm) was transferred to the mold. The mechanism works fully automatic and programmable. Gas controls, hydraulic die holder, solenoid valves and resistances are controlled by an auto-program. The materials (Greenpart-GP) are molded in dimensions of Ø35×5 mm. Afterwards, GP products were de-binding with solvent (in heptane solution) at 50°C for 3 h [27,32].

After molding and solvent de-binding, the materials were sintered under Ar gas flow in an atmosphere-controlled furnace. During the heat treatment, thermal de-binding (375°C/90 min) and sinter process (120 min) were applied to the products at once. The graphic describing the sinter process is given in Fig. 4. The heating rate was applied as 5°K/min until the thermal de-binding temperature. Up to sinter all temperatures, the heating rate is 8°K/min. [33]. At a constant temperature of 1050°C (30 min) for the development of the sintering process [34].

2.3. Characterization and in-vitro bio-corrosion process

Classical metallographic preparations have been made for the post-sinter materials applied according to Fig. 4. SEM images were taken from the surfaces after polishing and etching (immersion x3 HNO_3 and x1 HCl) [35]. SEM-EDX examinations were made on the images. Microstructures formed at different temperatures have been compiled. In addition, the surface image of the samples without post-sintering treatment and the fracture surface image formed under a press were also taken. Finally, density was measured according to Archimedes' principle and Vickers (HV) hardness values (average of five measurements) were taken [36]. In-vitro bio-corrosion analysis was carried out on the surfaces obtained in the biocompatibility stage of this study, in the artificial body solutions (hank's [37], saliva [38],

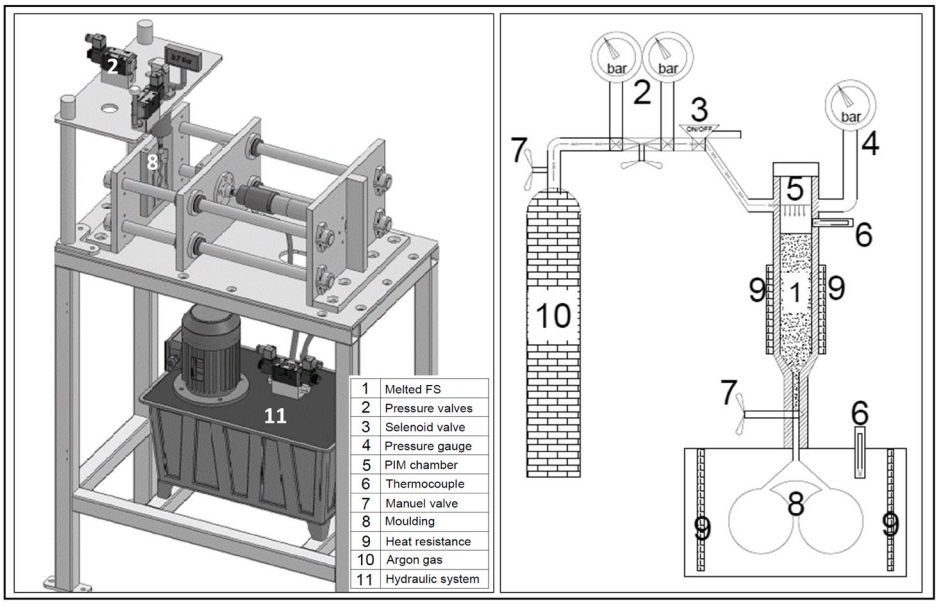

Fig. 3. Modified metal injection molding system

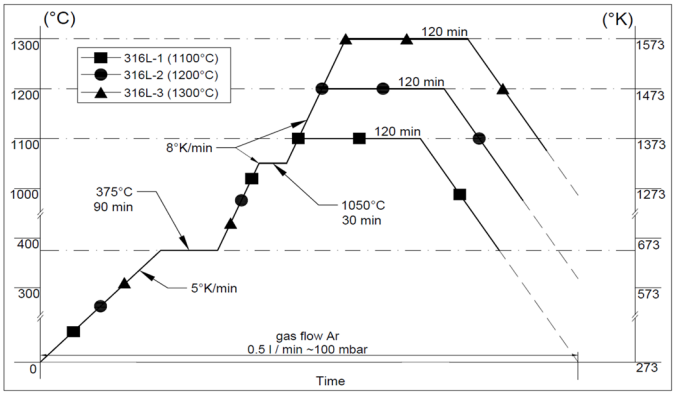

Fig. 4. Temperature and time diagram for sinter process

and 0.6M NaCl) given in TABLE 3. In the tests applied on the potentiostat and reference electrode cell, corrosion was applied in an area of 1 cm^2. Pt mesh electrode and Ag/AgCI reference electrode were used in the experiment. A salt bridge consisting of 3 M NaCl solution was employed for the corrosion experiments (for reference electrode). Anodic potential was observed in the scanning range of 1000 mV/-1500 mV. Corrosion rate (mm/y), E_{corr}, and I_{corr} values were recorded in the tests performed at room temperature [39-42].

TABLE 3

Chemical analyses for artificial body fluids and NaCl

g/L	Hank's	Saliva*	0.6M NaCl
NaCl	8	0.4	35
KCl	0.4	0.4	—
$CaCl_2$	0.14	0.795	—
Na_2HPO_4-$7H_2O$	0.09	—	—
$MgSO_4$-$7H_2O$	0.2	—	—
$NaHCO_3$	0.35	—	—
KH_2PO_4	0.06	—	—
$C_6H_{12}O_6$	1	—	—
Na_2S-$9H_2O$	—	0.005	—
$Na_2H_2PO_4$	—	0.69	—
KSCN	—	0.3	—
Urea	—	1	—
Distilled water	Balance	Balance	Balance

* To achieve pH (6.5), KOH, 0.1M HCl, and distilled water were added

Cytotoxicity biocompatibility test was applied to metallic samples after sintering. Firstly, extraction was made according to ISO 10993-12 standard [43]. L929 subcutaneous connective tissue cell (fibroblast) and American Type Collection (ATCC) were used as the cell line. In the culture mixture, Fetal Bovine Serum/Penicillin/Streptomycin was added on DMEM (1g/L glucose) + L-Glutamine + pyruvate. Samples are weighed according to the standard. Afterwards, it was kept in a water bath at 24 h/37°C/50 rpm parameters in a serum-free cell culture. Afterwards, the extraction was terminated, and the liquid was used within 24 h. In this experiment, cell culture medium was used as blank control, polyethylene as negative control and natural rubber as positive control.

In qualitative analysis, the cell cultures were planted in 96-well plates and expected to become confluent. Later, in an oven at 37°C and 5% CO_2, it was exposed to negative, positive control and sample extracts for 24 h. After the incubation, the cells were microscopically examined and evaluated according to the EN ISO 10993-5 standard [44,45].

In quantitative analysis, inoculation was performed in 96-well plates counting 10,000/well. After that, it was incubated for 24 h to provide 80% confluent. Then the cells; It was left in dilutions of the sample extract 1/1 to 1/64 (0.01 to 1) for 24 h. At the end of the process, the solution prepared as 1 mg/mL was added to the wells and the plates were kept in the oven for 3 h/37°C/5%CO_2. The experiment was terminated by adding isopropyl alcohol to the wells. The color change on the plates was measured in a spectrophotometer (570-650 nm) and the % viability values were calculated. The sample averages were proportioned to the negative control mean optical density values and expressed as % viability.

3. Results and discussion

3.1. Feedstock analyses

The graphic obtained because of the TGA applied to the FS structure is given in Fig. 5. 8% polymer (weight) content according to TGA plot showed approximate expected values. The previously detected single step weight change indicator of the PEG/PMMA prescription was repeated [27]. In this way, it is a known result that the polymer structure is removed without losing shape [27,30,31]. In this study, based on this, the thermal de-binding temperature was determined as 375°C.

3.2. Molding Specimens (Green part)

The flat and fracture surface images obtained from the products molded in the MIM system are given in Fig. 6. According

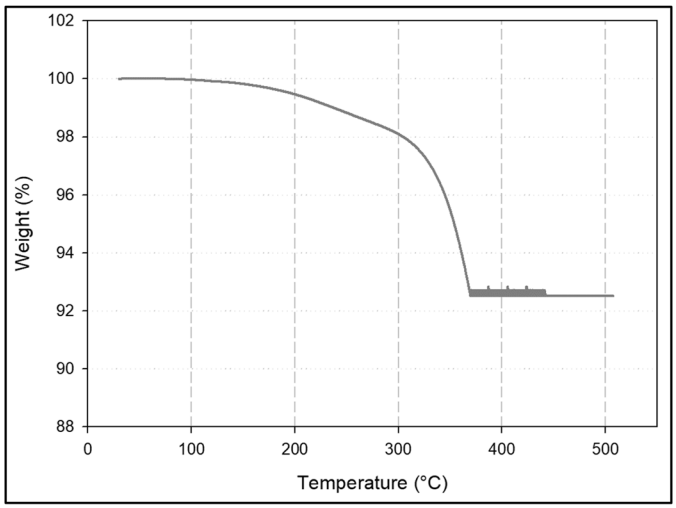

Fig. 5. TGA graph for feedstock

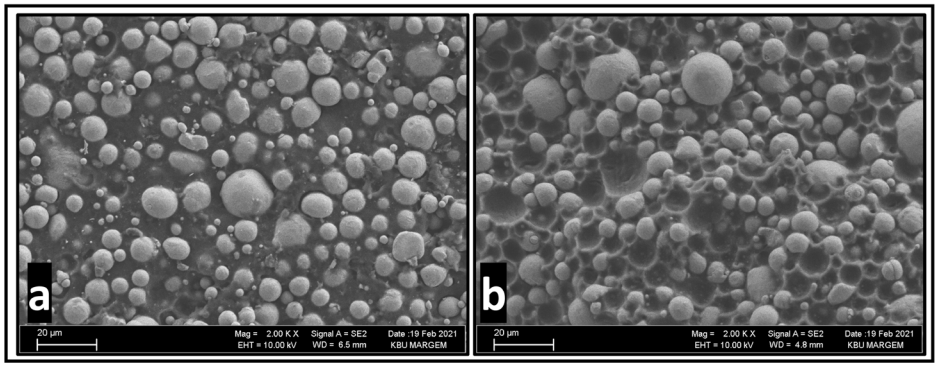

Fig. 6. Molded surface (a) and fracture surface (b)

to Fig. 6, polymer and particle distribution is homogeneous on both flat and fracture surfaces. It is observed that the polymer structure completely envelops the particles. In this structure, PMMA acts as a bone structure. PEG, on the other hand, fills the voids remaining in the filling structure. Distributions and images are like the literature [7,30,31].

3.3. Characterization for sinter parts

The microstructures of the materials with 2 h sinter applied at different temperatures are given in Fig. 7.

According to the study, as the sinter temperature increases, the microstructural morphology differs. At 1100°C, which is selected as the low temperature, shells were formed outside the particles. At an upper temperature (1200°C) the shells were dispersed, and the porosities increased. At the highest temperature (1300°C), the grains were completely formed. It is known that particle sizes increase due to the effect of sinter temperature and sinter time [32,46]. The development of the grains depends on the same variables [3,4,32,47]. In this study, when the microstructure (Fig. 7) details are examined, it is observed that the grain sizes tend to increase. According to the morphological changes of the microstructures, it is thought that the shell layers seen at low temperatures may be C and O, which are polymer wastes. Oxides are formed with the high affinity of oxygen and many elements [34,48,49]. Arifin et al according to his report, additions used during injection molding are known to leave oxide behind [50]. It is seen that oxide layers from polymer wastes leave the structure with the increase in temperature. EDX peaks and element ratios seen in Fig. 7 confirm this situation.

The surface and fracture surface obtained after sintering for the 316L-3 sample are shown in Fig. 8. On the sintered material surface (a) grain boundaries and gas outlet holes are clearly monitored. On the fracture surface (b), it is seen that the spherical dust grains course and turn into more angular structures. After the metallographic sample preparation, the same angular structures are like the picture in Fig. 7(c). It is known in the literature that spherical powders show diagonal structures after sintering [11,24,34,51].

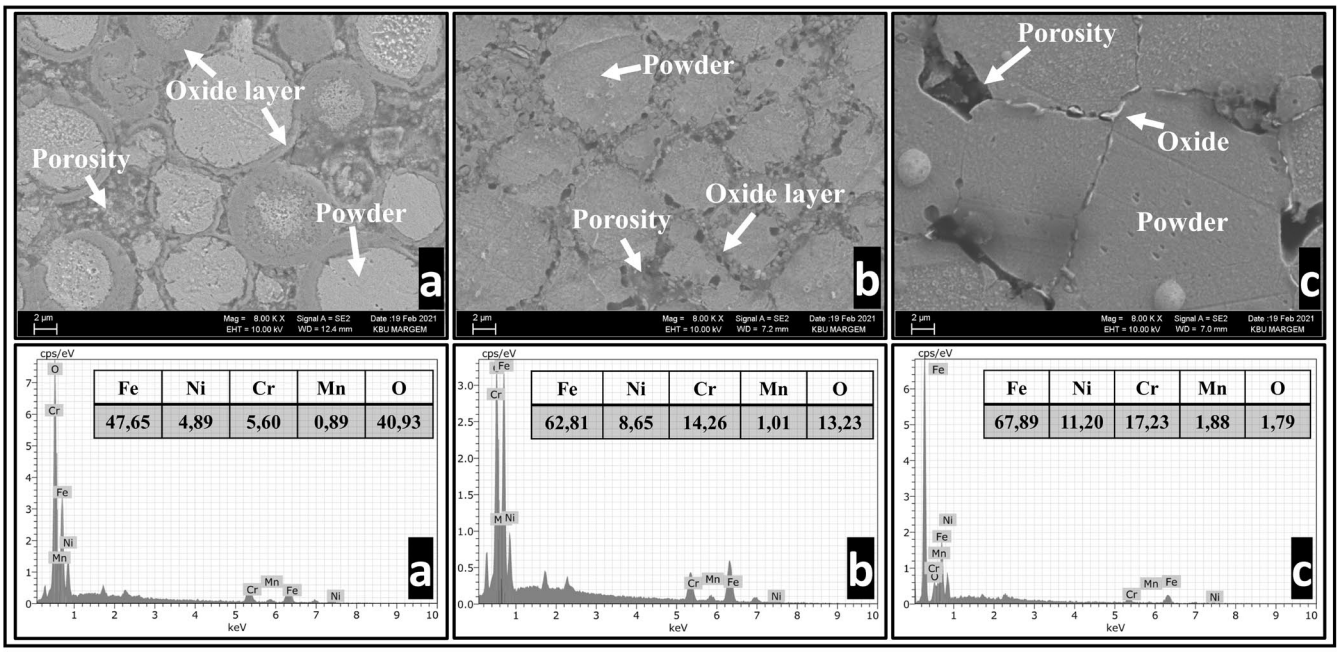

Fig. 7. Microstructures via SEM. (a) 316L-1, (b) 316L-2, and (c) 316L-3

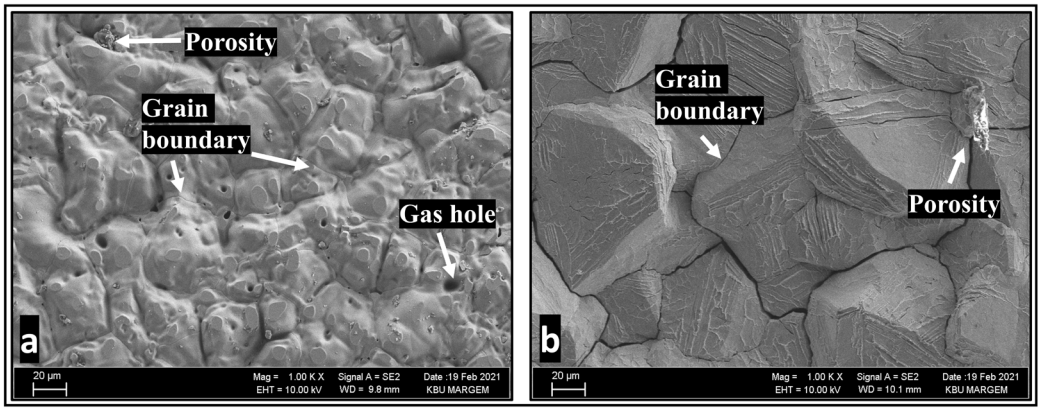

Fig. 8. Sintered part (1300°C) (a) surface and (b) sintered part fracture surface

The density values obtained from the injection stage to the sinter part are given in Fig. 9. Densities measured in air and water according to Archimedes' principle met the theoretical density values. During the solvent de-binding phase, PEG was removed from the structure and the density increased. As the sinter temperature increased, an increase in the density of the material was observed. As the amount of porosity in the structure decreases with the increase of the sinter temperature, the density has gained value positively [3,4,33]. Nykiel et al when examining the work done by the density; it was formed at 6.80 g/cm^3 levels as a result of sintering conditions of 1300°C/120 min [33]. In this study, density was measured as 6.74 g/cm^3 at the same sinter parameters.

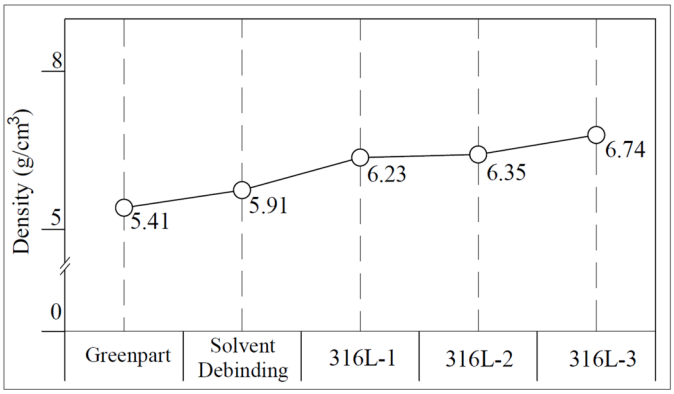

Fig. 9. Density values from start to finish

According to the hardness graph given in Fig. 10, as the sinter temperature increased, the hardness of the metallic structure increased. At low temperatures, impregnation and excess porosity had adverse effects on hardness. However, with the increase in temperature, the formation of the metallic structure increased the hardness value. Sintered results for PM 316L stainless steel are close to the literature values [9,20].

3.4. In-vitro bio-corrosion results

Metallic structures obtained because of sintering with a different production of 316L particles have been tested for corrosion in artificial body solutions. Tafel curves were obtained from potentiodynamic tests performed on Hank's and saliva solutions. Additionally, comparative experiments were carried out in 0.6 M NaCl solution The Tafel curves obtained after the corrosion test are given in Fig. 11.

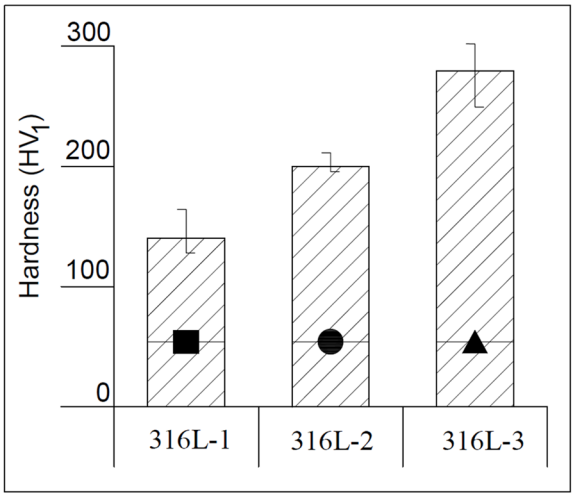

Fig. 10. Hardness results

Bio-corrosion experiments were carried out on samples that reached a metallic structure by sintering with temperature differences. The sample of 316L-3 (1300°C) showed low I_{corr} and low E_{corr} in all solutions. The fact that these variables are lower than other samples indicates that the corrosion resistance of the sinter part (316L-3) is high [52-54]. Especially the corrosion rate (obtained from the Gamry device) value and other data calculated over Tafel curves are given in TABLE 4. Based on the table and Tafel curves, it is observed that the resistance of the 316L-3 sample against bio-corrosion is high. Hou et al in the study by, I_{corr} values for 316L were found in the range of 0.271-4.669 µA [52]. In this study, the I_{corr} value was observed in the range of 0.0748-2.28 µA in the 316L-3 sample where the highest results were obtained. Thus, similar data with the literature were obtained because of bio-corrosion. In all calculations and solutions, the corrosion resistance of 316L-3 part was determined as the highest. The amount of porosity and oxide structures in sinter parts (316L-1 and 316L-2) made at values

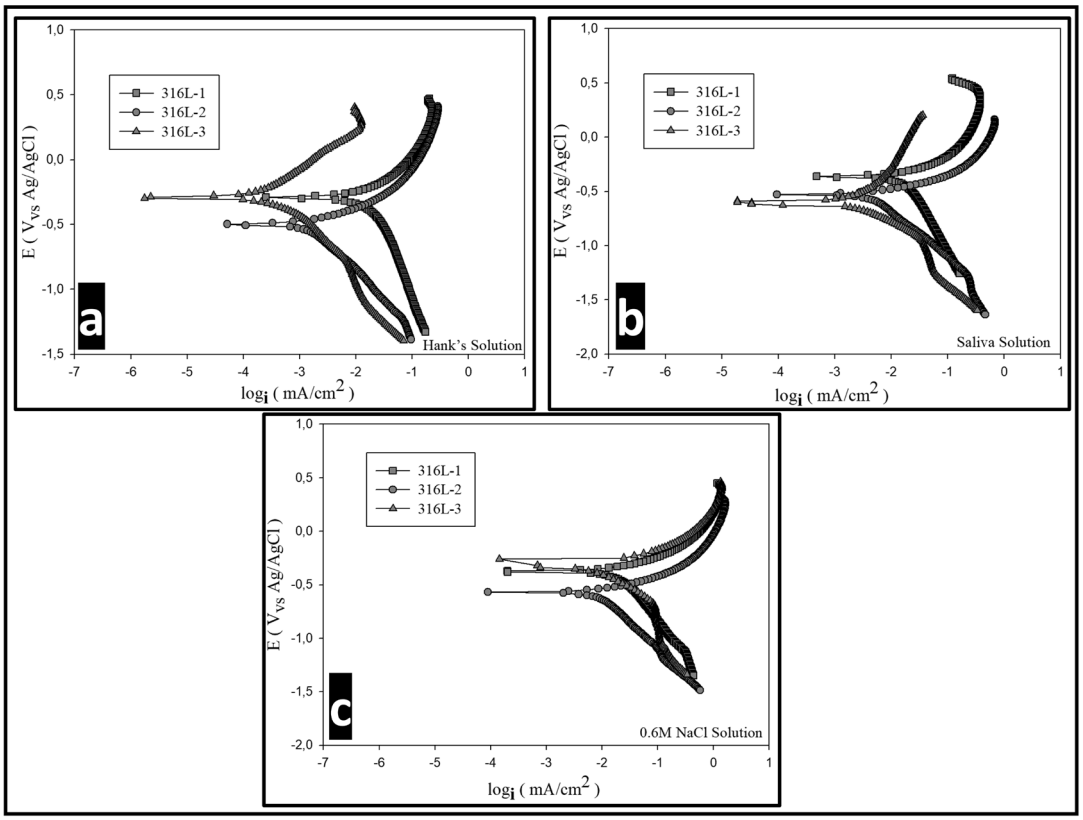

Fig. 11. Potentiodynamic polarization curves (Tafel curves) (a) Hank's, (b) Saliva, and (c) NaCl

TABLE 4

Potentiodynamic polarization curves data

Solution	Samples	I corr mA	E corr mV	Corrosion Rate (mm/y)
				Gamry device
Hank's	316L-1	0.0986	–287	15.60
	316L-2	0.00859	–496	1.402
	316L-3	0.0000748	–290	0.01708
Saliva	316L-1	0.364	–362	5.323
	316L-2	0.0236	–541	0.3449
	316L-3	0.000989	–596	0.02259
0.6 M NaCl	316L-1	0.157	–569	2.56
	316L-2	0.0157	–375	0.2568
	316L-3	0.00228	–225	0.05198

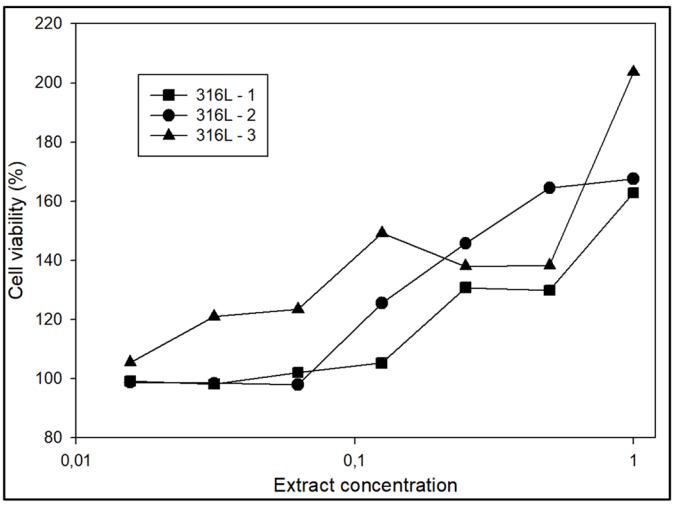

Fig. 12. Cell viability (%) rates for extract concentrations

lower than optimum temperature is high. With the effect of these parameters, it turns out that their corrosion resistance is low.

The % cell viability graph obtained according to the cytotoxicity results, which is a basic experiment on biocompatibility, is given in Fig. 12.

According to Fig. 12, as the concentration increased, the cell survival rate increased. As in other experiments, the most suitable sample at this stage was 316L-3 material. It is already known in practice and in the literature that 316L stainless steel series materials are biocompatible, in addition to many of their properties [10,55-58]. Afonso et al. the cell survival rate for 316L stainless steel (bulk material) was observed to be approximately 150% (50 to 125) in the study conducted by [55]. In this study, this ratio was approximately 103% (100 to 203) for 316L stainless steel (particle material). According to the relevant standard [43,44], the % vitality value should be at least 70%. With this comparison, the result is successful.

The images taken over the glass to monitor the cell survival rate are given in Fig. 13. Pictures were taken before and after the sample extracts were added. Cell proliferation is clearly observed in the pictures. When the % viability values and Fig. 13 are examined, it is seen that the materials are not toxic.

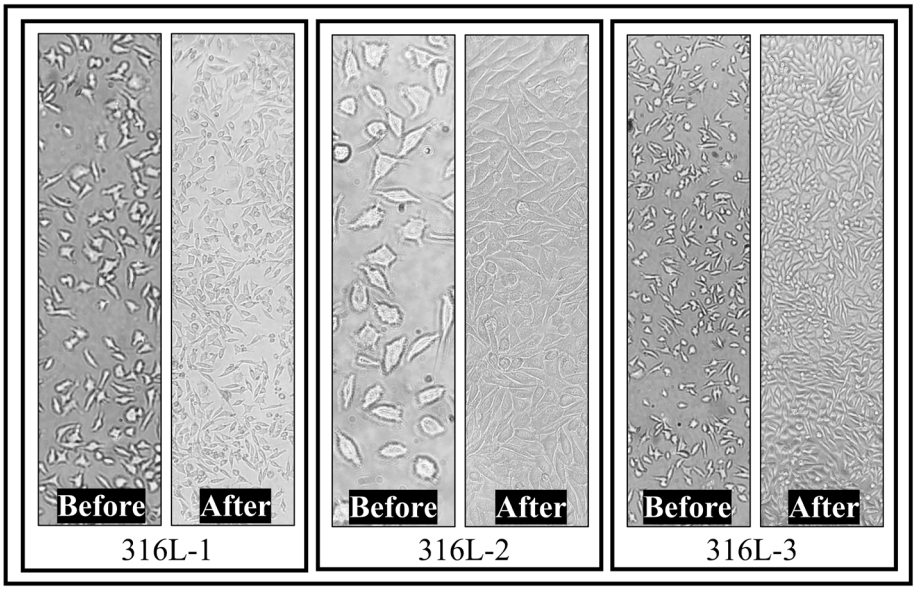

Fig. 13. Preparation images all MIM parts

4. Conclusions

Investigations for 316L alloy molded with a redesigned MIM method are compiled in this study. It has been seen that the oxygen level in the post-polymer structure, which is the main purpose of this study, does not affect the biocompatibility. The only and main result of this study is the use of the system in the production of biomaterials. Thus, a biocompatible stainless-steel alloy was produced within the framework of the following basic results.

1 – Metallic samples were produced in accordance with general MIM rules in the sinter part obtained with PEG/PMMA/SA polymer recipe.

2 – According to the microstructure results, the best metallic structure was obtained after 1300°C temperature and 2 h sintering.

3 – Density and hardness values measured after sintering show that a material complying with the general rules of powder metallurgy has been produced. For 316L grade stainless steel, 6.74 g/cm^3 and ~285 Hv_1 values were achieved, respectively.

4 – After the applied potentiodynamic corrosion, the data confirmed the biocompatibility of the stainless-steel alloy obtained. Corrosion resistance in the sintered sample (1300°C) reached 17.08e^{-3} mm/y values in artificial solutions.

5 – After the cytotoxicity test applied in the name of biocompatibility, it was observed that the rate of bacteria survival increased (vitality % 103) in the material sintered at high temperature (1300°C). With this result, biocompatibility has been confirmed.

Acknowledgement / Funding

Authors would like to thank the Karabuk University Scientific Project Unit (*FDK-2019-2106*) for financial support in the completion of this study.

Disclosure statement

No potential conflict of interest was reported by the authors.

REFERENCES

[1] R.M. German, Powder Metallurgy Science, 1984 Metal Powder Indust Feder, Wiley, USA.

[2] A. Salak, Ferrous Powder Metallurgy, Cambridge Int, 1995 Cambridge.

[3] S.C. Dhara, Sintering Characteristic of Precious Metal Powders, Particul. Sci. Technol. **11** (3-4), 207-227 (1993). DOI: https://doi.org/10.1080/02726359308906636

[4] R.M. German, Sintering Theory and Practice, 1996 Wiley, USA.

[5] R.M. German, Powder Injection Molding, 1990 Metal Powder Indust Feder, New Jersey, USA.

[6] R.M. German, K.F. Hens, S.-T.P. Lin, Key Issues in Powder Injection Molding, Am. Ceram. Soc. Bull. **70** (8), 1294-1302 (1991).

[7] T. Hartwig, G. Veltl, F. Petzoldt, H. Kunze, R. Scholl, B. Kieback, Powders for Metal Injection Molding, J. Eur. Ceram. Soc. **18** (9), 1211 (1998). DOI: https://doi.org/10.1016/S0955-2219(98)00044-2

[8] Z. Rak, New Trends in Powder Injection Moulding, Powder Metall. Met. C+ **38** (3-4), 126 (1998). DOI: https://doi.org/10.1007/BF02676037

[9] N. Kurgan, Y. Sun, B. Cicek, H. Ahlatci, Production of 316L Stainless Steel Implant Materials by Powder Metallurgy and Investigation of Their Wear Properties, Chin. Sci. Bull. **57** (15), 1873-1878 (2012). DOI: https://doi.org/10.1007/s11434-012-5022-5

[10] E. Salahinejad, M.J. Hadianfard, D.D. Macdonald, S. Sharifi-Asl, M. Mozafari, K.J. Walker, A.T. Rad, S.V. Madihally, L. Tayebi, In Vitro Electrochemical Corrosion and Cell Viability Studies on Nickel-Free Stainless Steel Orthopedic Implants, PLoS One **8** (4), e61633 (2013). DOI: https://doi.org/10.1371/journal.pone.0061633

[11] H. O. Gulsoy, S. Pazarlioglu, N. Gulsoy, B. Gundede, O. Mutlu, Effect of Zr, Nb and Ti Addition on Injection Molded 316l Stainless Steel for Bio-Applications: Mechanical, Electrochemical and Biocompatibility Properties, J. Mech. Behav. Biomed. Mater. **51**, 215-224 (2015). DOI: https://doi.org/10.1016/j.jmbbm.2015.07.016

[12] O. Balyts' kyi, Corrosion-Mechanical Characteristics of the Materials of Nonmagnetic Retaining Rings of Turbogenerators. Ii. High-Nitrogen 18mn−18cr Steels., Mater. Sci. **34** (1), 97-109 (1998). DOI: https://doi.org/10.1007/BF02362618

[13] O. Balyts' kyi, O. Krokhmal'nyi, Pitting Corrosion of 12kh18ag 18sh Steel in Chloride Solutions, Mater. Sci. **35** (3), 389-394 (1999). DOI: https://doi.org/10.1007/BF02355483

[14] N. Sezer, Z. Evis, S.M. Kayhan, A. Tahmasebifar, M. Koc, Review of Magnesium-Based Biomaterials and Their Applications, J. Magnes. Alloy. 23-36 (2018). DOI: https://doi.org/10.1016/j.jma.2018.02.003

[15] R.M. Pilliar, Metallic Biomaterials, in Biomedical Materials, 2021, Springer. p. 1-47.

[16] M. Schmidt, M. Goebeler, Nickel Allergies: Paying the Toll for Innate Immunity, J. Mol. Med. **89** (10), 961-970 (2011). DOI: https://doi.org/10.1007/s00109-011-0780-0

[17] Y. Zheng, X. Gu, F. Witte, Biodegradable Metals, Mater. Sci. Eng. R Rep. **77** 1-34 (2014). DOI: https://doi.org/10.1016/j.mser.2014.01.001

[18] Q. Chen, G.A. Thouas, Metallic Implant Biomaterials, Mater. Sci. Eng. R Rep. **87** 1-57 (2015). DOI: https://doi.org/10.1016/j.mser.2014.10.001

[19] F.O. Nestle, H. Speidel, M.O. Speidel, High Nickel Release from 1-and 2-Euro Coins, Nature **419** (6903), 132-132 (2002). DOI: https://doi.org/10.1038/419132a

[20] N. Kurgan, Effect of Porosity and Density on the Mechanical and Microstructural Properties of Sintered 316l Stainless Steel Implant Materials, Mater. Design **55**, 235-241 (2014). DOI: https://doi.org/10.1016/j.matdes.2013.09.058

[21] Y.-W. Kim, T. Mukarati, Fabrication and Shape Memory Characteristics of Highly Porous Ti-Nb-Mo Biomaterials, Arch. Metall. Mater. **62** (2017). DOI: https://doi.org/10.1515/amm-2017-0210

[22] K.-K. Wang, B.-J. Kim, S.-J. Jung, J.-W. Hwang, Y.-R. Kim, Fabrication and Characterization of Antimicrobial Surface-Modified Stainless Steel for Bio-Application, Surf. Coat. Technol. **310**, 256-262 (2017). DOI: https://doi.org/10.1016/j.surfcoat.2016.12.088

[23] C.V. Nayak, M. Ramesh, V. Desai, S.K. Samanta, Fabrication of Stainless Steel Based Composite by Metal Injection Moulding, Mater. Today **5** (2), 6805 (2018). DOI: https://doi.org/10.1016/j.matpr.2017.11.340

[24] R. German, Sintering: From Empirical Observations to Scientific Principles, 2014 Elsevier, United State of America.

[25] T. Senthilvelan, K. Raghukandan, A. Venkatraman, Testing and Quality Standards for Powder Metallurgy Products, Mater. Manuf. Process **18** (1), 105-112 (2003). DOI: https://doi.org/10.1081/AMP-120017592

[26] Y. Türen, Influence of Pressure Type on Powder Injection Moulding of Stainless Steel (316l) Powder, Hitite J. Sci. Eng. **4** (2), 85 (2017). DOI: https://doi.org/10.17350/HJSE19030000053

[27] B. Cicek, Y. Sun, Y. Turen, H. Ahlatci, Applicability of Different Powder and Polymer Recipes in a New Design Powder Injection Molding System, J. Polym. Eng. **41** (4), 299-309 (2021). DOI: https://doi.org/10.1515/polyeng-2020-0263

[28] B. Cicek, Y. Sun, Y. Turen, H. Ahlatci, Investigation of Microstructural Evolution of Gas-Assisted Metal Injection Molded and Sintered Mg-0.5 Ca Alloy, Sci. Sinter. **54** (1), 25-37 (2022). DOI: https://doi.org/10.2298/SOS2201025C

[29] T.Y. Chan, S.T. Lin, Effects of Stearic Acid on the Injection Molding of Alumina, J. Am. Ceram. Soc. **78** (10), 2746-2752 (1995). DOI: https://doi.org/10.1111/j.1151-2916.1995.tb08050.x

[30] H. Bakan, Y. Jumadi, P. Messer, H. Davies, B. Ellis, Study of Processing Parameters for Mim Feedstock Based on Composite Peg-Pmma Binder, Powder Metall. **41** (4), 289 (1998). DOI: https://doi.org/10.1179/pom.1998.41.4.289

[31] M. Omar, H. Davies, P. Messer, B. Ellis, The Influence of Pmma Content on the Properties of 316l Stainless Steel Mim Compact, J. Mater. Process Tech. **113** (1-3), 477 (2001). DOI: https://doi.org/10.1016/S0924-0136(01)00641-0

[32] D.-Y. Wi, Y.-K. Kim, T.-S. Yoon, K.-A. Lee, Microstructure and High Temperature Oxidation Properties of Fe-Cr-Ni Hk30 Alloy Manufactured by Metal Injection Molding, Arch. Metall. Mater. **64** (2019). DOI: https://doi.org/10.24425/amm.2019.127571

[33] A. Szewczyk-Nykiel, R. Bogucki, Sinter-Bonding of Aisi 316l and 17-4 Ph Stainless Steels, J. Mater. Eng. Perform. **27** (10), 5271-5279 (2018). DOI: https://doi.org/10.1007/s11665-018-3590-5

[34] J.-P. Choi, G.-Y. Lee, J.-I. Song, W.-S. Lee, J.-S. Lee, Sintering Behavior of 316l Stainless Steel Micro-Nanopowder Compact Fabricated by Powder Injection Molding, Powder Technol. **279**, 196-202 (2015). DOI: https://doi.org/10.1016/j.powtec.2015.04.014

[35] P.N. Rao, D. Kunzru, Fabrication of Microchannels on Stainless Steel by Wet Chemical Etching, J. Micromech. Microeng. **17** (12), N99 (2007). DOI: https://doi.org/10.1088/0960-1317/17/12/N01

[36] E. Standard, ISO 6507-1: 2007. Metallic Materials. Vickers Hardness Test, in International Organization for Standardization, Geneva. 2007.

[37] H. Jia, X. Feng, Y. Yang, Effect of Grain Morphology on the Degradation Behavior of Mg-4 Wt% Zn Alloy in Hank's Solution, Mater. Sci. Eng. C **106**, 110013 (2020). DOI: https://doi.org/10.1016/j.msec.2019.110013

[38] J. Pytko-Polonczyk, A. Jakubik, A. Przeklasa-Bierowiec, B. Muszynska, Artificial Saliva and Its Use in Biological Experiments, J. Physiol. Pharmacol. **68** (6), 807-813 (2017).

[39] S.D. Cramer, B.S. Covino, Asm Handbook Vol. 13 a Corrosion: Fundamentals, Testing, and Protection, 2003 ASM International, Materials Park, OH.

[40] Z. Shi, M. Liu, A. Atrens, Measurement of the Corrosion Rate of Magnesium Alloys Using Tafel Extrapolation, Corros. Sci. **52** (2), 579-588 (2010). DOI: https://doi.org/10.1016/j.corsci.2009.10.016

[41] S. Cengiz, A. Uzunoglu, L. Stanciu, M. Tarakci, Y. Gencer, Direct Fabrication of Crystalline Hydroxyapatite Coating on Zirconium

by Single-Step Plasma Electrolytic Oxidation Process, Surf. Coat. Technol. **301**, 74-79 (2016).
DOI: https://doi.org/10.1016/j.surfcoat.2015.12.069

[42] S. Cengiz, A. Uzunoglu, S. M. Huang, L. Stanciu, M. Tarakci, Y. Gencer, An in-Vitro Study: The Effect of Surface Properties on Bioactivity of the Oxide Layer Fabricated on Zr Substrate by Peo, Surf. Interfaces **22**, 100884 (2021).
DOI: https://doi.org/10.1016/j.surfin.2020.100884

[43] U.T. Seyfert, V. Biehl, J. Schenk, In Vitro Hemocompatibility Testing of Biomaterials According to the Iso 10993-4, Biomol. Eng. **19** (2-6), 91-96 (2002).
DOI: https://doi.org/10.1016/S1389-0344(02)00015-1

[44] R.F. Wallin, E. Arscott, A Practical Guide to ISO 10993-5: Cytotoxicity, Med. Device Diagn. Ind. **20**, 96-98 (1998).

[45] M. Gonsior, R. Kustosz, M. Kościelniak-Ziemniak, T. Wierzchoń, Biocompatible Evaluation of Biomaterials Used in the New Polish Extracorporeal Pulsatile Heart Assist Device Religaheart Ext, Arch. Metall. Mater. **60** (2015).
DOI: https://doi.org/10.1515/amm-2015-0374

[46] Ö. Özgün, H.Ö. Gülsoy, R. Yılmaz, F. Fındık, Microstructural and Mechanical Characterization of Injection Molded 718 Superalloy Powders, J. Alloys Compd. **576**, 140-153 (2013).
DOI: https://doi.org/10.1016/j.jallcom.2013.04.042

[47] J.L. Johnson, L.K. Tan, P. Suri, R.M. German, Mechanical Properties and Corrosion Resistance of Mim Ni-Based Superalloys, Proceedings of the 2004 International Conference on Powder Metallurgy and Particulate Materials, Princeton, USA, Citeseer, (2004) 89-101.

[48] K. Anderson, J. Groza, M. Fendorf, C. Echer, Surface Oxide Debonding in Field Assisted Powder Sintering, Mat. Sci. Eng. A-Struct. **270** (2), 278 (1999).
DOI: https://doi.org/10.1016/S0921-5093(99)00197-5

[49] H. Takeda, K. Nakano, N. Tanibata, M. Nakayama, Novel Mg-Ion Conductive Oxide of M-Cordierite Mg0. 6al1. 2si1. 8o6, Sci. Technol. Adv. Mater. **21** (1), 131 (2020).
DOI: https://doi.org/10.1080/14686996.2020.1730237

[50] A. Arifin, A.B. Sulong, N. Muhamad, J. Syarif, M.I. Ramli, Powder Injection Molding of Ha/Ti6al4v Composite Using Palm Stearin as Based Binder for Implant Material, Mater. Design **65**, 1028-1034 (2015).
DOI: https://doi.org/10.1016/j.matdes.2014.10.039

[51] M.B. Shongwe, I.M. Makena, M.M. Ramakokovhu, T. Langa, P.A. Olubambi, Sintering Behavior and Effect of Ternary Additions on the Microstructure and Mechanical Properties of Ni–Fe-Based Alloy, Part. Sci. Technol. **36** (5), 643-654 (2018).
DOI: https://doi.org/10.1080/02726351.2017.1298686

[52] X. Hou, Q. Ren, Y. Yang, X. Cao, J. Hu, C. Zhang, H. Deng, D. Yu, K. Li, W. Lan, Effect of Temperature on the Electrochemical Pitting Corrosion Behavior of 316l Stainless Steel in Chloride-Containing Mdea Solution, J. Nat. Gas Sci. Eng. **86**, 103718 (2021). DOI: https://doi.org/10.1016/j.jngse.2020.103718

[53] B. Çiçek, Y. Sun, A Study on the Mechanical and Corrosion Properties of Lead Added Magnesium Alloys, Mater. Design **37**, 369-372 (2012). DOI: https://doi.org/10.1016/j.matdes.2012.01.029

[54] J. Qiu, A. Wu, Y. Li, Y. Xu, R. Scarlat, D.D. Macdonald, Galvanic Corrosion of Type 316l Stainless Steel and Graphite in Molten Fluoride Salt, Corros. Sci. **170**, 108677 (2020).
DOI: https://doi.org/10.1016/j.corsci.2020.108677

[55] M.L.d.A. Afonso, R.F. Jaimes, P.A. Nascente, S.O. Rogero, S.M. Agostinho, Surface Characterization, Electrochemical Behaviour and Cytotoxicity of Uns S31254 Stainless Steel for Orthopaedic Applications, Mater. Lett. **148**, 71-75 (2015).
DOI: https://doi.org/10.1016/j.matlet.2015.01.157

[56] M. Speidel, New Nitrogen-Bearing Austenitic Stainless Steels with High Strength and Ductility, Met. Sci. Heat Treat. **47** (2005).
DOI: UDC 669.14.018.8:669.786

[57] V. Pokhmurs'kyi, O. Balyts'kyi, O. Krokhmal'nyi, General and Pitting Corrosion of Chromium-Manganese Steels in Halogen Solutions, Mater. Sci. **36** (3), 313-324 (2000).
DOI: https://doi.org/10.1007/BF02769592

[58] O. Balyts'kyi, I. Kostyuk, Strength of Welded Joints of Cr-Mn Steels with Elevated Content of Nitrogen in Hydrogen-Containing Media, Mater. Sci. **45** (1), 97-107 (2009).
DOI: https://doi.org/10.1007/s11003-009-9166-7